ROKVISS – Robotics Component Verification on ISS

Current Experimental Results on Parameter Identification

1 Abstract

ROKVISS, a new space robotics technology experiment, was successfully installed outside at the Russian Service Module of the International Space Station (ISS) during an extravehicular space walk at the end of January 2005. Since February 2005 a two joint manipulator can be operated from ground via a direct radio link. The aim of ROKVISS is the in flight verification of highly integrated modular robotic joints as well as the demonstration of different control modes, reaching from high system autonomy to force feedback teleoperation. A main goal of the experiment is the evaluation of the dynamical parameters (especially friction, motor constant and stiffness), as well as the monitoring of their evolution over the duration of the mission, in order to validate the long term performance of the system. The paper gives first a short overview of the experiment and in particular a description of the applied control structures. The main focus of the paper is on the joint parameter identification results obtained so far, during eight months of operation.

2 General Experiment Description

After ROTEX (the first remotely controlled space robot on board of the shuttle COLUMBIA), ROKVISS is the second space robot experiment proposed and realised by DLR's Institute of Robotics and Mechatronics (DLR-RM) in cooperation with the German space companies EADS-ST, Kaiser-Threde, and vHS (von Hörner & Sulger) with close collaboration of the Russian Federal Space Agency ROSKOSMOS and RKK Energia. While the project was started in 2002, the ROKVISS hardware was mounted outside at the Russian Service Module of the ISS in January 2005 (Fig. 2). Since February 2005 ROKVISS is operated by DLR-RM, close supported by ZUP, the ISS ground station in Moscow.

The ROKVISS experiment consists of a small robot with two torque-controlled joints (Fig. 3), mounted on an Universal Workplate (UWP), a controller, a stereo camera, an illumination system, an earth observation camera, a power supply, and a mechanical contour device for verifying the robot's functions and performance (Fig. 1). These two robot joints have been extensively tested and the joint parameters have been identified by repetitively performing predefined robot tasks in an automatic mode, or based on direct operator interaction. The automatic mode is necessary due to the fact that communication constraints limit the direct link experiment time to windows of only up to seven minutes length, when the ISS passes over the tracking station German Space Operations Center (GSOC).

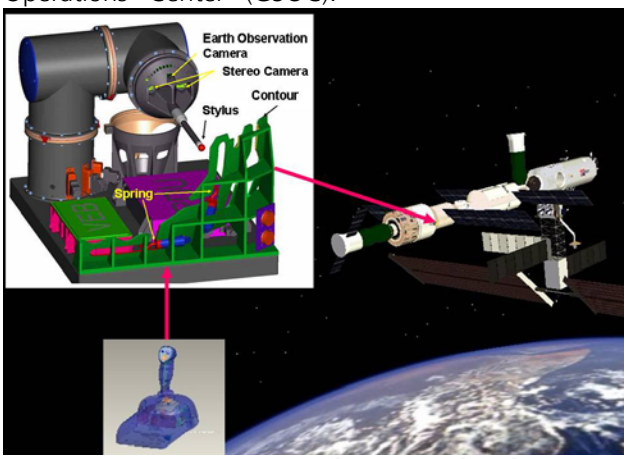

Fig. 1 ROKVISS manipilator with the contour following environment

Fig. 2 At the end of a 5 hours space walk the astronauts succeeded in mounting ROKVISS and connecting the necessary cables.

The main goals of the ROKVISS [2] experiment are:
the **verification of DLR's modular light-weight, torque-controlled robotic joints** in outer space, under realistic mission conditions, and the identification of their dynamic and friction behaviour over time [12],[13]; The joints are based on DLR's new high energy motor ROBODRIVE and they are identical to those used in DLR's seven joint light weight robot. This technology is the basis for our future "robonaut" developments.

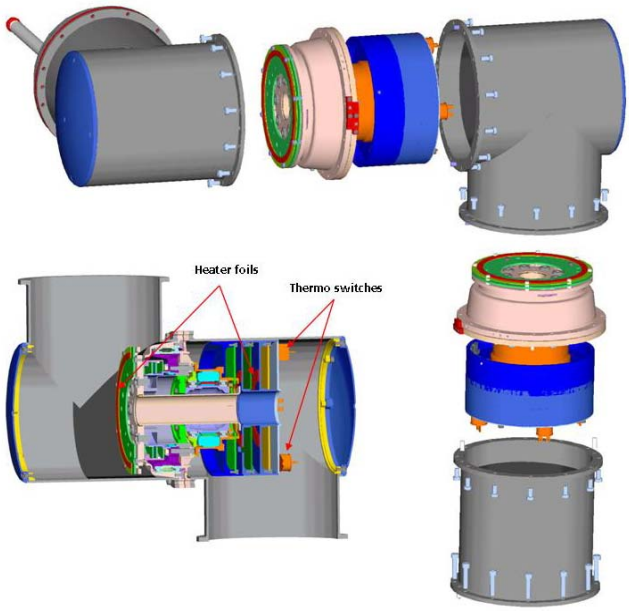

Fig. 3 The two joint ROKVISS manipulator

the verification of force-reflecting telemanipulation to show the **feasibility of telepresence methods** [3],[4] for future satellite servicing tasks, as we are convinced that the inclusion of the human ground operator into the control loop is a must in many situations (Fig. 4).

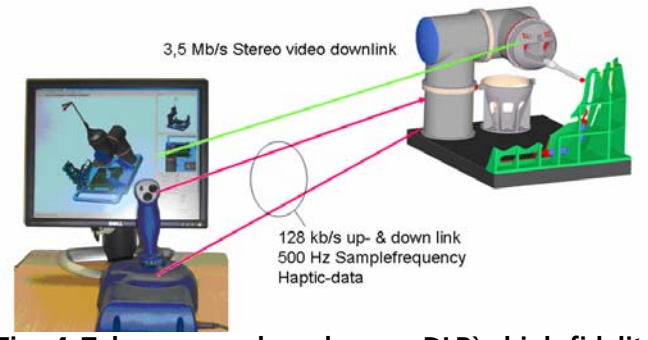

Fig. 4 Telepresence based upon DLR`s high-fidelity force reflecting joystick and stereo visual feedback

Detailed information about the system setup and the telepresence experiments can be found in [1]. In the next chapter, the paper gives a short description of the controller structure of the robot. The rest of the paper is dedicated to the presentation and discussion of the parameter identification results obtained during the first eight months of operation.

3 Controller Structure

The controller structures have initially been developed and verified on the basis of the DLR light-weight robots of generation II and III [5]. In particular a flexible-joint model is assumed. Fast and reliable methods for the identification of the joint model parameters (joint stiffness, damping and friction) were developed, while the rigid body parameters are directly generated from the mechanical CAD programs [6],[7]. This lead to an accurate simulation of the robot dynamics on ground, so that it was possible to develop and test the controller structures in the simulation first.

The basic joint level controller is a joint state feedback controller with compensation of gravity and friction [8]. The state vector contains the motor position, the joint torques, as well as their derivatives. By the appropriate parameterisation of the feedback gains, the controller structure can be used to implement position, torque or impedance control. The gains of the controller can be computed in every Cartesian cycle, based on the desired joint stiffness and damping, as well as depending on the actual value of the inertia matrix. Hence, this controller structure fulfils the following functionalities:

It provides active vibration damping of the flexible joint structure;

It maximises the bandwidth of the joint control for the given instantaneous values of the inertia matrix;

It implements variable joint stiffness and damping.

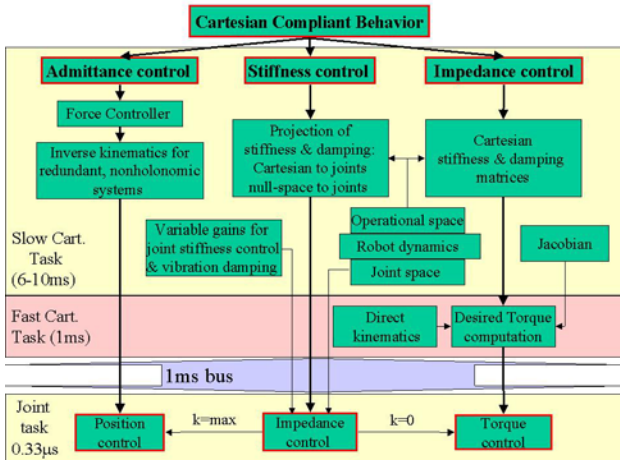

Fig. 5 Controller architecture

Based on this joint control structure, three different strategies for implementing Cartesian compliant motion have been realised (Fig. 5): admittance control, which accesses the joint position interface through the inverse kinematics; impedance control, which is based on the joint torque interface; and Cartesian stiffness control, which accesses the joint impedance controller [9].

The position controller as well as the impedance controller is based on a passivity approach under consideration of the joint flexibilities [10],[11]. A physical interpretation of the joint torque feedback loop has been given as the shaping of the motor's kinetic energy, while the implementation of the desired stiffness can be regarded as shaping of potential energy. Therefore, the Cartesian impedance controller can be designed and analyzed within a passivity based framework in the same manner as the joint state feedback controller. This constitutes a new, unified approach for the torque, impedance and position control on both joint and Cartesian level.

An important advantage of these passivity-based controllers is the robustness with respect to uncertainties of the robot or load parameters, as well as to contact-situations with unknown but passive environments.

Despite of the fact that the Cartesian controllers are of very limited practical use for a two dof robot, the entire control structure of the DLR light-weight robots has been implemented also for the ROKVISS system, in order to validate the software for further missions, for robots with six or seven dof.

4 Joint parameter identification results

For the dynamical model of the robot we assume the well known flexible joint model proposed in [14]:

$$\tau_m = J\ddot{q}_1 + \tau + DK^{-1}\dot{\tau} + \tau_F$$

$$\tau + DK^{-1}\dot{\tau} = M(q_2)\ddot{q}_2 + C(q_2,\dot{q}_2)\dot{q}_2 + g(q_2)$$

$$\tau = K(q_1 - q_2)$$

where τ_m is the motor torque vector, q_1 and q_2 are the motor and link positions respectively, and τ is the joint torque. J is the motor inertia matrix and K and D are the elasticity and damping matrices, determined mainly by the harmonic drive gear and the torque sensor. M, C and g are the same as for rigid robots: the mass matrix, the Coriolis and centripetal torque vector and the gravity vector. The latter has to be considered of course only during terrestrial test. τ_F is the friction torque vector. The following friction model was initially used:

$$\tau_F = (\tau_C + \mu|\tau|)\mathrm{sign}(\dot{q}_1) + d_1\dot{q}_1$$

where τ_C and μ are the coefficients of constant and torque-dependent Coulomb friction respectively, and d_1 is the viscous friction coefficient. The motors are operated in current control mode and the motor torque is related to the current I trough the motor constant k_m:

$$\tau_m = k_m^{-1} I$$

By using 3D CAD programs for the mechanical design, the problem of determining the parameters of the rigid robot dynamics becomes straightforward, since they can be generated with high accuracy from the design data. This of course requires a detailed modelling of all components, including motors, gears and electronics.
The parameters which still have to be identified are the friction parameters, the motor constant and the joint stiffness.
To identify the different parameter groups we perform dedicated measurements which enable independent identification for each group. This procedure avoids complex online optimization problems which, in our earlier experiments, always resulted in local minima, very different form the real physical parameters.

4.1 Friction identification

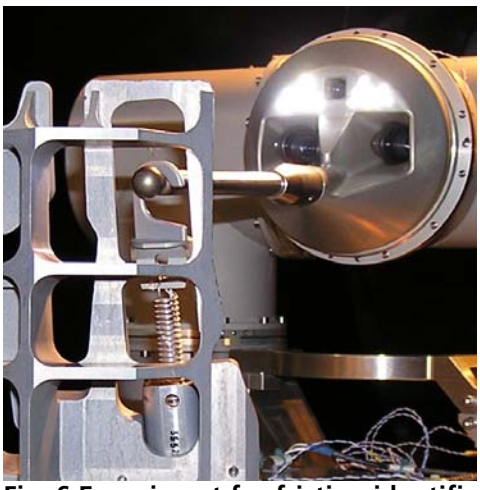

Fig. 6 Experiment for friction identification: Pulling a spring with different constant velocities.

For the identification of the motor side friction the following signals are available: the commanded motor current, the measured motor position and hence, by differentiation, the motor velocity and acceleration, as well as the measured joint torque. The identification procedure determines the motor torque constant k_m, the Coulomb friction τ_C, the friction coefficient for the load dependent component μ, and the viscous friction coefficient d_1. The identification of these parameters can be formulated as a static, linear optimization problem. This means that for a properly chosen trajectory, which independently excites all parameters, a fast and reliable parameter convergence can be obtained. Such a trajectory is given when pulling the springs of the test setup using a saw-tooth trajectory with different constant velocities (Fig. 6). Due to the variable load torque, the reversion of the movement direction, and the coverage of the entire velocity range, all parameters are well excited.

4.1.1 Results for joint 2

Typical identification plots for joint 2 are given in Fig. 7 and Fig. 8. Fig. 7 contains a reference measurement on ground while Fig. 8 shows a typical measurement in space. The corresponding numerical results for the friction values are given in Table 1 and Table 2.
One can see that the viscous friction has a nonlinear component on ground. An extension of the model by higher order viscous friction terms is required in order to capture these effects. This extension is introduced in the next chapter for the parameter identification of joint 1. Surprising is the fact that the viscous friction is very low (actually negligible) in the space experiments for joint 2. For this reason, the simple, linear viscous model was used also for the on ground measurement for joint 2 despite of the imperfect fit, in order to enable a more realistic comparison of the on-ground and on-orbit values.
In order to test the reliability of the identified values, the motor constant k_m was also identified on a separate motor test-bed and the optimization was performed only

for the remaining parameters. Table 1 and Table 2 show that the results for the two cases are quite similar, and for the on-orbit measurement almost identical.

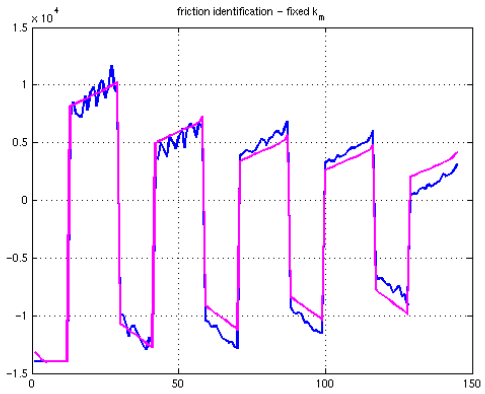

Fig. 7 Commanded current and current estimation after the identification of the friction parameters. The movements are performed with 40.0, 20.0, 10.0, 5.0, and 1.0deg/s. Joint 2, at 02.11.2004 (reference on ground).

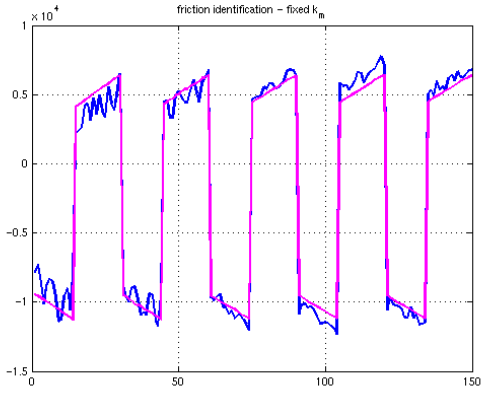

Fig. 8 Commanded current and current estimation after the identification of the friction parameters. The movements are performed with 40.0, 20.0, 10.0, 5.0, and 1.0deg/s. Joint 2, at 08.06.2005 (on orbit).

Table 1 Friction parameters of joint 2 on ground.

	with fixed k_m	with optimized k_m
k_m [Nm/inc]	330.28	364.7
τ_c [Nm]	13.69	13.15
μ []	0.229	0.0985
d_1 [Nms/rad]	28.96	26.99

Table 2 Friction parameters of joint 2 in space.

	with fixed k_m	with optimized k_m
k_m [Nm/inc]	330.28	330.08
τ_c [Nm]	22.02	21.98
μ []	0.0	0.0
d_1 [Nms/rad]	0.0	0.0

4.1.2 Time and temperature dependency for joint 2

In order to evaluate the evolution of the friction parameters over the operation time and with the temperature, the same experiment is repeated several times every month. Fig. 9 shows the evolution over time of the friction values at a velocity of 5deg/s. The plot emphasizes also the contribution of the different friction components.
The total friction is almost velocity independent and is only slightly higher than the average friction on ground
Compared to the ground measurement, the total friction in joint 2 increased only by a factor of about 20% in space and was rather constant during operation time.
A heating system is used to regulate the operating temperatures on-orbit between -20°C and +30°C. Within this range, the temperature dependency of the parameters is also rather low and lies close to the range of the identification uncertainty (Fig. 16).

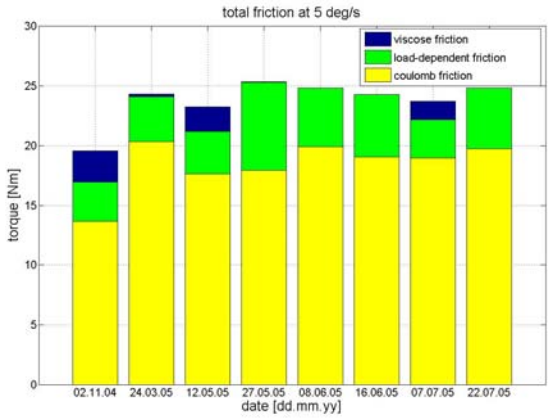

Fig. 9 Time evolution of total friction at a speed of 5deg/s. The first bar corresponds to the reference measurement on ground.

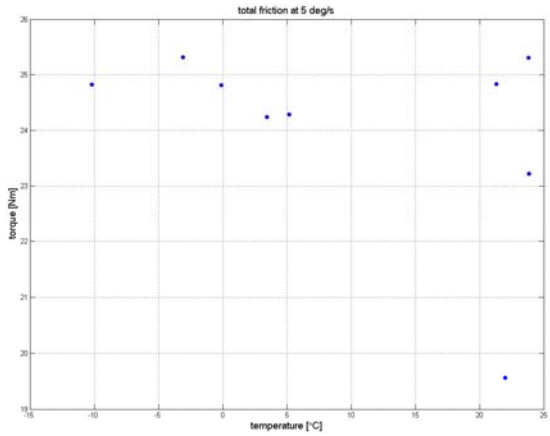

Fig. 10 Total friction at 5deg/s, plotted over the temperature. The isolated value corresponds to the reference measurement on ground.

4.1.3 Results for joint 1

The results for the friction identification for joint 1 on ground are very similar to those from joint 2. A nonlinear dependency on the velocity can be seen in Fig. 11, which is insufficiently captured by the linear viscous model. Therefore, a third order polynomial is used alternatively to model the viscous friction behaviour:

$$\tau_F = (\tau_C + \mu|\tau| + d_2\dot{q}_1^2)\text{sign}(\dot{q}_1) + d_1\dot{q}_1 + d_3\dot{q}_1^3$$

The fitting with this extended model is considerably better (Fig. 12). Table 3 compares the parameters for the two approaches. For the model with higher complexity, also the Coulomb friction, which can be seen as the zero order coefficient of the polynomial, has a lower value, since part of the friction force is distributed to the other components.

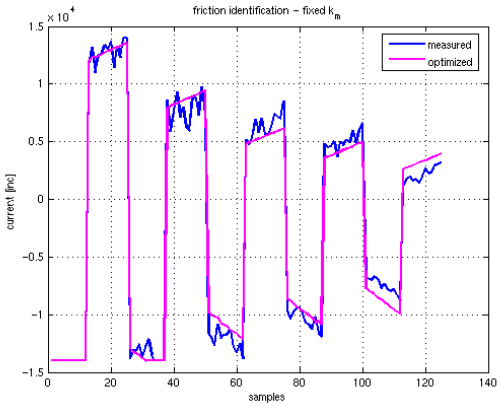

Fig. 11 Commanded current and current estimation after the identification of the friction parameters. The movements are performed with 30.0, 20.0, 10.0, 5.0, and 1.0deg/s. Joint 1, on 02.11.2004 (reference on ground). Here, only a linear viscous friction component is considered.

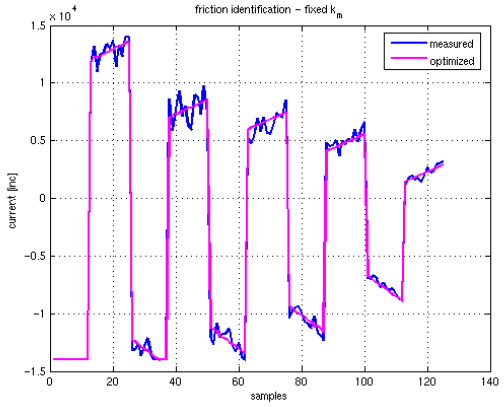

Fig. 12 Commanded current and current estimation after the identification of the friction parameters. The movements are performed with 30.0, 20.0, 10.0, 5.0, and 1.0deg/s. Joint 1, on 02.11.2004 (reference on ground). Here, the velocity dependency is modelled by a third order polynomial.

Table 3 Friction parameters of joint 1 on ground.

	Linear viscous friction (Fig. 11)	Cubic viscous friction (Fig. 12)
k_m [Nm/inc]	345.62	345.62
τ_C [Nm]	12.37	7.62
μ []	0.300	0.272
d_1 [Nms/rad]	42.08	150.49
d_2 [Nms^2/rad^2]	0.0	-403.67
d_3 [Nms^3/rad^3]	0.0	370.3830

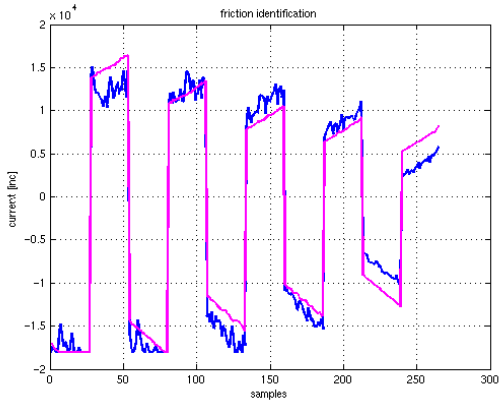

Fig. 13 Commanded current and current estimation after the identification of the friction parameters. The movements are performed with 30.0, 20.0, 10.0, 5.0, and 1.0deg/s. Joint 1, at 07.07.2005 (on orbit). Here, only a linear viscous friction component is considered.

For joint 1, the shape of the friction in space looks very similar to that on ground. Fig. 13 and Fig. 14 show the corresponding identification results for linear and cubic viscous friction. The numerical values are shown in Table

4. Compared to the values from Table 3, it can be seen that the friction, in particular the Coulomb friction increased considerably. Therefore, the upper motor current limit was increased in order to provide a similar load torque range.

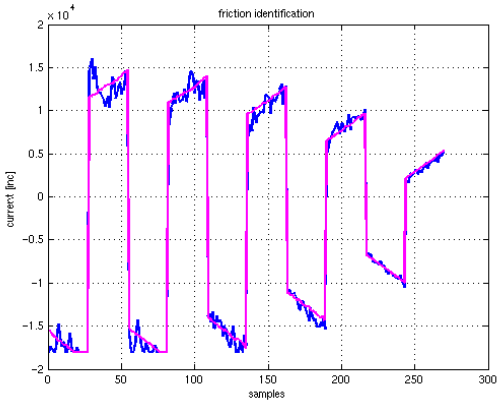

Fig. 14 Commanded current and current estimation after the identification of the friction parameters. The movements are performed with 30.0, 20.0, 10.0, 5.0, and 1.0deg/s. Joint 1, at 07.07.2005 (on orbit) Here, the velocity dependency is modelled by a third order polynomial.

Table 4 Friction parameters of joint 1 in space.

	Linear viscous friction (Fig. 13)	Cubic viscous friction (Fig. 14)
k_m [Nm/inc]	345.62	345.62
τ_C [Nm]	22.57	13.00
μ []	0.187	0.0162
d_1 [Nms/rad]	49.82	250.1
d_2[Nms^2/rad^2]	0.0	-690.4
d_3[Nms^3/rad^3]	0.0	627.3

4.1.4 Time and temperature dependency for joint 1

The preliminary results of the on-orbit identification show that the total friction for joint 1 in space increased by about 50% compared to the friction on ground, taken at 20°C, under normal atmospheric pressure. However, only o small further degradation of the parameters can be observed so far over the first eight months of operation (Fig. 15). This suggests the conclusion that the lubricant changed its properties in an early mission stage during the check-out phase and afterwards reached a quite stable operating condition.
The temperature dependency of the parameters is also rather low and lies close to the range of the identification uncertainty (Fig. 16).

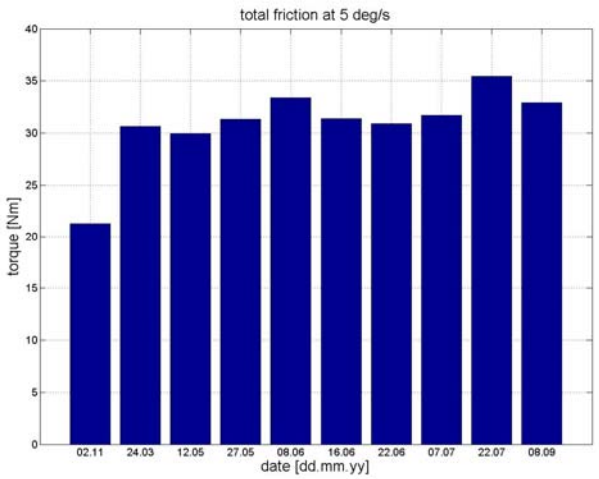

Fig. 15 Time evolution of total friction at a speed of 5deg/s. The first bar corresponds to the reference measurement on ground.

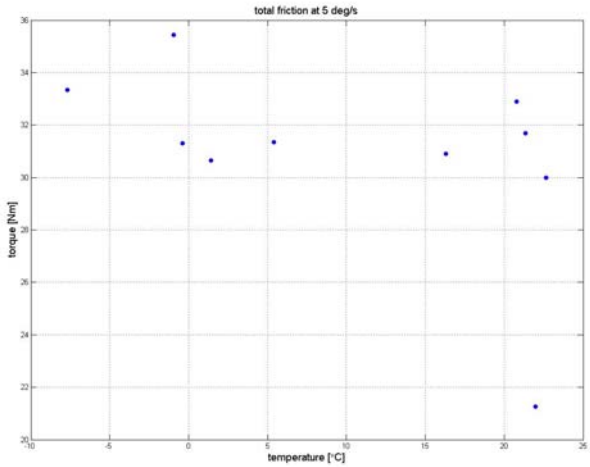

Fig. 16 Total friction at 5deg/s, plotted over the temperature. The isolated value corresponds to the reference measurement on ground.

4.2 Conclusions for friction identification

As a conclusion for the friction identification, the following can be stated:
The friction in the two joints increased initially, already at the first experiment in space compared to the values on ground, but remained afterwards rather constant.
All the controllers were robust with respect to these changes
The friction change of joint 1 and joint 2 is different. While friction in joint 1 has the same structure as on ground, but with values increased by 50%, for the friction in joint 2 there is no more significant viscous friction and the total increase of friction is lower (about 20%). Since the same lubricant was used for both joints, further experiments are needed in order to explain the different behaviour.

In order to provide a better fit of measured simulation data, a nonlinear (third order polynomial) is required. However, due to the higher number of optimization parameters, their variance over different experiments is higher. A trajectory with a higher number of distinct velocities is needed in order to reduce the variance of the results. This will be done within a software update during the second phase of the mission.

5 Stiffness Identification

The main sources of elasticity in the joints are the flex splines of the harmonic drives and the torque sensors. The elasticity is identified by contacting a rigid surface with the tip of the robot and by commanding a slowly changing force to the joints. Since the torque is measured after the gear-box, the stiffness can be easily identified with the available torque and position signal. The model torque is computed as a product of position increment and stiffness.

A typical identification result can be seen in Fig. 17 and Fig. 18. The stiffness for joint 2 has values around 4900 Nm/rad in space. As expected, there are no very significant differences between the stiffness values on ground and in space. Still, a change of about 15% can be observed. However this deviation is in the range of the load dependent stiffness variation and the controllers are designed to be robust with respect to such uncertainties.

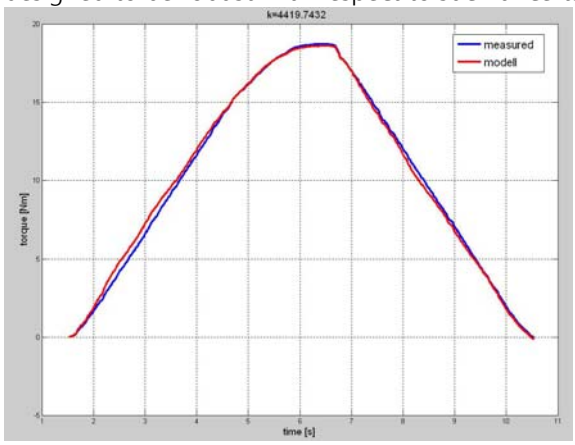

Fig. 17 Result of stiffness optimization for joint2 on ground.

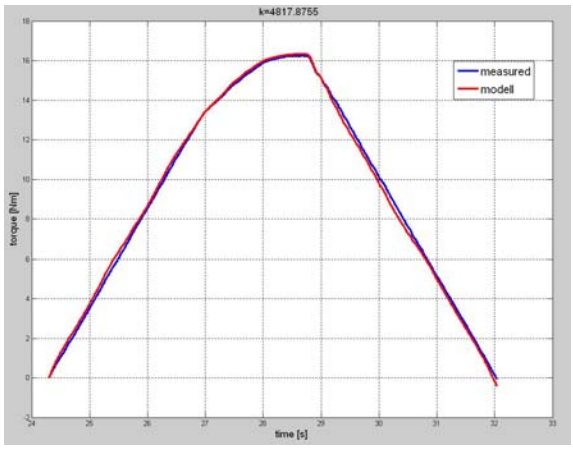

Fig. 18 Result of stiffness optimization for joint2 in space.

6 Conclusions

Though the ROKVISS mission is planed for at least one year, already now – i.e. after 8 months of operation – the main goals of the mission have been achieved. The hardware proved to work reliably under space conditions. The dynamical parameters of the joints, although somewhat different then on ground, have a small variation over time and with temperature. The controller structures proved to be robust with respect to these variations.

The majority of the developed hardware and the results of the experiments will be taken into account for the design of a more complex free-flying robotic system (e.g. 7-axis robot) intended to be used in an On Orbit Servicing (OSS) technology experiment (TECSAS) in which a non cooperative target shall be approached, captured and finally de-orbited.

REFERENCES

[1] G. Hirzinger , K. Landzettel , D. Reintsema, C. Preusche, A. Albu-Schäffer, B. Rebele, M. Turk: ROKVISS – Robotics Component Verification on ISS. Proc. of 'The 8th Int. Symposium on Artifical Intelligence, Robotics and Automation in Space - iSAIRAS', Munich, Germany. (2005)

[2] Landzettel, K., Brunner, B., Lampariello, R., Preusche, C., Reintsema, G., et al.: System Prerequisites and Operational Modes for On Orbit Servicing. Proc. ISTS International Symposium on Space Technology and Science, Miyazaki, Japan, May 30-June 6, 2004, Proceedings, (2004)

[3] Preusche, C., Reintsema, D., Landzettel, K., Fischer, M., Hirzinger, G.: DLR on the way towards Telepresent On-Orbit Servicing. Proc. Mechatronics & Robotics 2004, (2004)

[4] Preusche, C., Reintsema, D., Landzettel, K., Hirzinger, G.: ROKVISS - towards Telepresence Control in Advanced Space Missions. Proc. 3rd. International Conference on Humanoid Robots (Humanoids 2003), Munich and Karlsruhe, Oct. 2003, (2003)

[5] G. Hirzinger, N. Sporer, A. Albu-Schäffer, M. Hähnle, R. Krenn, A. Pascucci, M. Schedl: DLR's torque-controlled light weight robot III - are we reaching the technological limits now?, Proc. IEEE International Conference on Robotics and Automation ICRA, pp. 1710-1716, (2002)

[6] Albu-Schäffer, A.: Regelung von Robotern mit elastischen Gelenken am Beispiel der DLR-Leichtbauarme. Doctoral thesis, TU München, (2002)

[7] A. Albu-Schäffer, G. Hirzinger: Parameter identification and passivity based joint control for a 7DOF torque controlled light weight robot, in: Proc.

Int. Conf. on Robotics and Automation, Seoul, Korea, pp. 1087-1093 (2001)
[8] Albu-Schäffer, A., Hirzinger, G.: A globally stable state feedback controller for flexible joint robots. Advanced Robotics, Special Issue, Vol. 15, No. 8, (2001), pp.799-814
[9] Albu-Schäffer, A., Hirzinger, G.: Cartesian Impedance Control Techniques for Torque Controlled Light Weight Robots. Proc. IEEE International Conference on Robotics and Automation, Washington D.C, USA, pp.657-663, (2002)
[10] Albu-Schäffer, A., Ott, C., Hirzinger, G.: A Passivity Based Cartesian Impedance Controller for Flexible Joint Robots – Part II: Full State Feedback, Impedance Design and Experiments. Proc. IEEE International Conference on Robotics and Automation ICRA, New Orleans, USA, April 26 - May 1, pp.2666-2672, (2004)
[11] Ott, C., Albu-Schäffer, A., Kugi, A., Stramigioli, S., Hirzinger, G.: A Passivity Based Cartesian Impedance Controller for Flexible Joint Robots – Part I: Torque Feedback and Gravity Compensation. Proc. IEEE International Conference on Robotics and Automation ICRA, New Orleans, USA, April 26 - May 1, pp.2659-2665, (2004)
[12] Schäfer, B., Landzettel, K., Albu-Schäffer, A., Hirzinger, G.: ROKVISS: Orbital Testbed for Tele-Presence Experiments, Novel Robotic Components and Dynamics Models Verification. Proc. 8th ESA Workshop on Advanced Space Technologies for Robotics and Automation (ASTRA), Noordwijk, The Netherlands, Nov. 2-4, (2004)
[13] Schäfer, B., Rebele, B., Landzettel, K.: ROKVISS - Space Robotics Dynamics and Control Performance Experiments at the ISS. Proc. ACA2004 IFAC Symposium on Automatic Control in Aerospace, St . Petersburg, Russia, 13-18 June 2004, pp.333-338, (2004)
[14] Spong, M.: Modeling and Control of Elastic Joint Robots. IEEE Journal of Robo- tics and Automation, RA-3(4):291-300, 1987.